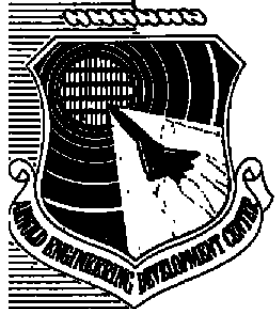


For



Computation of Three-Dimensional Time-Dependent Flow Using the Euler Equations

J. L. Jacobs and K. R. Kneile
ARO, Inc.

July 1981

Final Report for Period October 1, 1979 — September 30, 1980

Approved for public release; distribution unlimited.

**ARNOLD ENGINEERING DEVELOPMENT CENTER
ARNOLD AIR FORCE STATION, TENNESSEE
AIR FORCE SYSTEMS COMMAND
UNITED STATES AIR FORCE**

NOTICES

When U. S. Government drawings, specifications, or other data are used for any purpose other than a definitely related Government procurement operation, the Government thereby incurs no responsibility nor any obligation whatsoever, and the fact that the Government may have formulated, furnished, or in any way supplied the said drawings, specifications, or other data, is not to be regarded by implication or otherwise, or in any manner licensing the holder or any other person or corporation, or conveying any rights or permission to manufacture, use, or sell any patented invention that may in any way be related thereto.

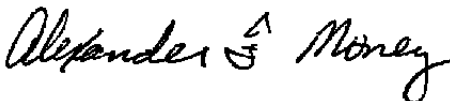
Qualified users may obtain copies of this report from the Defense Technical Information Center.

References to named commercial products in this report are not to be considered in any sense as an indorsement of the product by the United States Air Force or the Government.

This report has been reviewed by the Office of Public Affairs (PA) and is releasable to the National Technical Information Service (NTIS). At NTIS, it will be available to the general public, including foreign nations.

APPROVAL STATEMENT

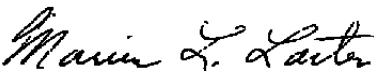
This report has been reviewed and approved.



ALEXANDER F. MONEY
Aeronautical Systems Division
Deputy for Operations

Approved for publication:

FOR THE COMMANDER



MARION L. LASTER
Director of Technology
Deputy for Operations

UNCLASSIFIED

REPORT DOCUMENTATION PAGE		READ INSTRUCTIONS BEFORE COMPLETING FORM
1 REPORT NUMBER AEDC-TR-80-49	2 GOVT ACCESSION NO.	3 RECIPIENT'S CATALOG NUMBER
4 TITLE (and Subtitle) COMPUTATION OF THREE-DIMENSIONAL TIME-DEPENDENT FLOW USING THE EULER EQUATIONS		5 TYPE OF REPORT & PERIOD COVERED Final Report, Oct. 1, 1979 - Sept. 30, 1980
		6 PERFORMING ORG. REPORT NUMBER
7 AUTHOR(s) J. L. Jacocks and K. R. Kneile, ARO, Inc., a Sverdrup Corporation Company		8 CONTRACT OR GRANT NUMBER(s)
9 PERFORMING ORGANIZATION NAME AND ADDRESS Arnold Engineering Development Center/DOT Air Force Systems Command Arnold Air Force Station, Tennessee 37389		10 PROGRAM ELEMENT, PROJECT, TASK AREA & WORK UNIT NUMBERS Program Element 65807F
11 CONTROLLING OFFICE NAME AND ADDRESS Arnold Engineering Development Center/DOS Air Force Systems Command Arnold Air Force Station, Tennessee 37389		12 REPORT DATE July 1981
		13 NUMBER OF PAGES 40
14 MONITORING AGENCY NAME & ADDRESS (if different from Controlling Office)		15. SECURITY CLASS (of this report) UNCLASSIFIED
		15a. DECLASSIFICATION/DOWNGRADING SCHEDULE N/A
16 DISTRIBUTION STATEMENT (of this Report) Approved for public release; distribution unlimited.		
17 DISTRIBUTION STATEMENT (of the abstract entered in Block 20, if different from Report)		
18 SUPPLEMENTARY NOTES Available in Defense Technical Information Center (DTIC).		
19 KEY WORDS (Continue on reverse side if necessary and identify by block number) computer programs transonic flow Cartesian coordinates three dimensional flow algorithms		
20 ABSTRACT (Continue on reverse side if necessary and identify by block number) The development of a computer program to solve the three-dimensional, unsteady Euler equations is described. A finite volume method in Cartesian coordinates is used with the MacCormack predictor-corrector algorithm. The grid imposed on the computational domain is topologically equivalent to a regular grid on a cube. The resulting control volumes are hexahedrons with		

UNCLASSIFIED

UNCLASSIFIED

20. ABSTRACT (Continued)

quadrilateral faces. Solutions are presented to show the accuracy of the computer program and to demonstrate the degree of flexibility with respect to complex model geometry.

UNCLASSIFIED

PREFACE

The work reported herein was conducted by the Arnold Engineering Development Center (AEDC), Air Force Systems Command (AFSC). The Air Force project manager was Elton R. Thompson, DOT. The results of the research were obtained by ARO, Inc., AEDC Group (a Sverdrup Corporation Company), operating contractor for the AEDC, AFSC, Arnold Air Force Station, Tennessee, under ARO Project No. P32A-01. The manuscript was submitted for publication on September 16, 1980.

The authors acknowledge the support and contributions of W. E. Dietz, T. L. Donegan, R. R. Jones, K. R. Stansbury, T. W. Swafford, and D. L. Whitfield in demonstrating the accuracy and flexibility of the computer program.

CONTENTS

	<u>Page</u>
1.0 INTRODUCTION	5
2.0 NUMERICAL METHOD	
2.1 Euler Equations	5
2.2 Computational Mesh	6
2.3 Solution Algorithm	7
2.4 Boundary and Initial Conditions	8
2.5 Smoothing	9
2.6 Code Structure and Timing Studies	10
3.0 RESULTS AND DISCUSSION	11
4.0 CONCLUDING REMARKS	14
REFERENCES	15

ILLUSTRATIONS

Figure

1. Computational Mesh Nomenclature	17
2. Computation of Flow over a Double-Wedge with Orthogonal Mesh	18
3. Computation of Flow over a Double-Wedge with Inclined Mesh	20
4. Effect of Smoothing	22
5. Computation of Flow over a Cone at Angle of Attack	23
6. Computation of Flow over an Ogive-Cylinder at Angle of Attack	25
7. Computation of Flow over a Three-Store Cluster at Zero Angle of Attack	26
8. Computation of Flow over a Lifting Airfoil	28
9. Computation of Flow over an Aircraft Forebody	32
10. Computation of Flow within a Wind Tunnel Contraction	33
11. Computation of Flow within an Aircraft Inlet	34
12. Computation of Flow about a Hollow-Nose Probe	35
13. Computation of Unsteady Flow	37
14. Computation of Counter-Flowing Jets	38
 NOMENCLATURE	 39

1.0 INTRODUCTION

Recent success has been demonstrated in the difficult area of computing transonic, three-dimensional inviscid flow fields over complex configurations. Notable is the work of Jameson and Caughey (Refs. 1 through 3) for solution of the full potential equations with wing-body configurations, and Boppe (Ref. 4) for solution of the small-perturbation-potential equations with wing-body-pylon-nacelle configurations. Another major contribution is evident in the work of Cline (Ref. 5), who solved the axisymmetric Euler equations for convergent-divergent nozzle configurations. Although as yet unpublished, Phares of ARO, Inc., has extended the Cline code to three-dimensional nozzle configurations.

These computer programs are used routinely at AEDC to resolve problems and to enhance the ground test capabilities of the wind tunnel and engine test facilities. Because many situations arise for which the available codes are not applicable, it was deemed necessary to write a new computer program with as few limitations as possible. Specifically, there were to be no geometry restrictions, and the code should be capable of treating both internal and external configurations without the assumptions of irrotational or isoenergetic flow.

This report describes the development of a computer program (designated ARO-1) to solve the three-dimensional, unsteady Euler equations in Cartesian coordinates using a finite volume (volume flux) approach. The basic numerical algorithm is the explicit predictor-corrector scheme of MacCormack (Ref. 6). Some results are compared with exact solutions to illustrate the basic accuracy of the code, whereas other solutions are presented to demonstrate the great flexibility available with respect to geometry and extreme flow situations.

2.0 NUMERICAL METHOD

2.1 EULER EQUATIONS

The three-dimensional, unsteady Euler equations are conservatively written in Cartesian coordinates as

$$\frac{\partial G}{\partial t} + \nabla \cdot F = 0 \quad (1)$$

where

$$G = \begin{bmatrix} \rho \\ \rho u \\ \rho v \\ \rho w \\ e \end{bmatrix} \quad F = \begin{bmatrix} \rho u & \rho v & \rho w \\ \rho u^2 + P & \rho uv & \rho uw \\ \rho uv & \rho v^2 + P & \rho vw \\ \rho uw & \rho vw & \rho w^2 + P \\ (e + P)u & (e + P)v & (e + P)w \end{bmatrix} \quad (2)$$

and the pressure is given by

$$P = (\gamma - 1) \left[e - \frac{1}{2} \rho (u^2 + v^2 + w^2) \right] \quad (3)$$

All variables are dimensionless, with the reference conditions usually taken to be free-stream density and sound speed, the latter given by

$$c = \left(\frac{\gamma P}{\rho} \right)^{1/2} \quad (4)$$

Integrating Eq. (1) over a small stationary volume, V , yields

$$\frac{\partial}{\partial t} \int_V G dV + \int_V \nabla \cdot F dV = 0 \quad (5)$$

Using the mean value and divergence theorems results in

$$\frac{\partial G}{\partial t} = - \frac{1}{V} \int_S n \cdot F dS \quad (6)$$

where n is the outward unit normal to the surface, S , enclosing V , and G is associated with some point interior to the volume (taken to be the volume center for practical purposes).

2.2 COMPUTATIONAL MESH

The grid imposed on the computational flow region is topologically equivalent to a regular grid on a cube. The resulting control volumes are hexahedrons with quadrilateral faces which are not necessarily planar. Degenerate volumes may also be used; for example, two edges may coincide to form a distorted triangular prism, thereby maintaining flexibility with respect to arbitrary geometry. A representative control volume within the mesh is shown in Fig. 1. Three pairs of opposite faces are evident and denoted by subscripts $k = 1$,

2, or 3. One of the eight vertices is designated as the positive corner, and the area vectors of the three faces meeting at the vertex are designated by S_1^+ , S_2^+ , and S_3^+ . The other three faces have area vectors designated by S_1^- , S_2^- , and S_3^- , respectively. When two volume elements share a common face, that face is represented by S_k^+ in one volume and S_k^- in the other. This coupling forms three "pseudo directions" through the computational mesh and permits selection of three indices for cataloging the flow variable independent of the mesh orientation with respect to the coordinate axes.

The area vector is computed as one-half the cross product of the diagonal vectors. The resulting direction is an "average" normal over the surface with the magnitude being the projected area in that direction. This vector is resolved into Cartesian components. Center points are defined by simple averaging; the center point coordinates of each face are the average of the four vertex coordinates, and the coordinate of the volume center is the average of the eight vertex coordinates. A center vector is defined as the vector directed from the volume center to the center of a face. The volume of each hexahedron is calculated as one-third the sum of the dot products of the center and area vectors.

Routines for mesh generation are user-supplied. Several examples of usable computational meshes are given in Section 3.0. The only restriction with respect to mesh coordinates is that they be consistently ordered so that the resulting volume calculation is positive. Negative volumes indicate either errors in constructing the mesh or simply a reversal of one of the coordinate indices.

2.3 SOLUTION ALGORITHM

The basic numerical algorithm is the explicit predictor-corrector method of MacCormack (Ref. 6). The flux integral in Eq. (6) is approximated by summing the scalar products of the area vectors and the appropriately evaluated flux vectors. The solution can be advanced from time n to $n+1$ using

$$\begin{aligned}\bar{G}^{n+1} &= G^n - \frac{\omega \Delta t}{V} \left(\sum_k \bar{F} \cdot S_k^+ + \sum_k \bar{F}^- \cdot S_k^- \right) \\ G^{n+1} &= \frac{1}{2\omega} \bar{G}^{n+1} + \left(1 - \frac{1}{2\omega} \right) G^n \\ &\quad - \frac{\Delta t}{2V} \left(\sum_k \bar{F}^+ \cdot S_k + \sum_k \bar{F}^- \cdot S_k^- \right)\end{aligned}\tag{7}$$

where F is the flux vector evaluated at the volume center, F^+ is the flux vector evaluated at the center point of the volume sharing the S_k^+ face, and F^- similarly corresponds with S_k^- . The overbar represents evaluation at the predictor time. Pressure is updated using Eq. (3) and boundary conditions applied at the end of both predictor and corrector steps. The orientation of the predictor-corrector is changed each time step by cycling the positive corner among the eight vertices.

The parameter, ω , was introduced in Eq. (7) to help stabilize the algorithm. For $\omega = 1$, the scheme reduces to the volume flux form of the MacCormack algorithm. Increasing ω increases the truncation error, which acts as an artificial viscosity, thereby smoothing the results. Increasing ω also rigorously reduces the order of accuracy from second order to first order. However, for an irregular computational mesh the algorithm is less than second-order accurate even with $\omega = 1$.

The time step, Δt , is limited in magnitude by the Courant-Friedrich-Lewy stability criterion. The maximum allowable time step is computed as the minimum of

$$\Delta t = \frac{V}{|q \cdot S| + c |S|} \quad (8)$$

over the entire mesh for each face of each volume where q is the velocity vector. Preliminary experience indicates that the time step must be further reduced by $\sqrt{\omega}$ for stability. Since the sound speed, c , requires a square-root operation, Δt is calculated only every 128th time step to reduce computer time.

2.4 BOUNDARY AND INITIAL CONDITIONS

Boundary conditions are applied by using phantom points exterior from the computational mesh. When the properties such as upstream free-stream conditions are known, these values are specified at the phantom points.

Mirror conditions are used at planes of symmetry. Pressure, density, and energy at the phantom points are equated to the neighboring interior values. The velocity vector is mirrored using

$$q_{bc} = q_{in} - 2 \left(\frac{S \cdot q_{in}}{S \cdot S} \right) S \quad (9)$$

where q_{in} is the velocity vector neighboring the phantom point, q_{bc} , and S is the boundary area vector.

At wall or body surface boundaries, mirror conditions are also generally used. This results in inaccuracies when the boundaries are not planar; however, no efficient method of implementing a normal momentum equation or characteristic-type boundary condition has been developed for arbitrary surface geometry. The magnitude of the errors introduced by the mirror assumption is discussed in Section 3.0.

Outflow or outer boundaries are treated with either the first or second differences of all variables set to zero. In general, zero gradient conditions obtained by equating the phantom points to the neighboring interior values have proved to be more stable than zero second difference conditions.

Initial conditions for exterior-type flows are usually taken to be free-stream values with body surface boundary conditions impulsively applied at time zero. For interior flows the initial conditions are usually obtained from one-dimensional isentropic flow relations with the velocity vector aligned with the mesh. Subsonic duct flow solutions also use an upstream boundary condition which is similar to that of Cline (Ref. 5), derived from characteristic relations with pressure specified at the outflow boundary.

2.5 SMOOTHING

During development of the code it became very evident that the basic algorithm is unconditionally unstable when applied to an irregular mesh. Some form of artificial viscosity is required to damp the high frequency truncation errors and to dissipate expansion shocks which are admissible (Ref. 7). Three types of smoothing have been used.

The “omega factor” (ω) introduced in Eq. (7) is a viable method of favorably increasing the truncation error to add artificial viscosity. Its primary advantage is the addition of stability with minimal impact on efficiency. However, the omega factor has been rarely used during the code evaluation for two reasons: (1) aesthetically, it seems incorrect to reduce the formal accuracy of a numerical scheme, and more to the point, (2) the production version of the computer program contained a coding error relative to the omega factor.

Some solutions have been obtained using the third-order smoothing of Ref. 8. This procedure specifically evaluates the third-order truncation errors and includes them in evaluation of the surface flux integral over each volume element. Although stability is assured and the solutions are accurate, the computation time is significantly increased relative to the basic algorithm.

The majority of solutions have been obtained using explicit weighted averaging. At each eighth time step, the entire flow field is smoothed by simple averaging of adjacent volume elements, with the central element being weighted by the factor

$$W = 20 \left(\frac{V}{V_{\min}} \right)^{1/3} \quad (10)$$

where V_{\min} represents the minimum of volume V over the computational domain. After averaging, the smoothed interior values are used to update boundary conditions.

2.6 CODE STRUCTURE AND TIMING STUDIES

The basic code consists of six subroutines which accomplish the following tasks:

1. DTCAL computes the maximum allowable time step.
2. BC applies boundary conditions.
3. FLUXX evaluates surface fluxes in the $k = 1$ direction.
4. FLUXY evaluates surfaces fluxes in the $k = 2$ direction.
5. FLUXZ evaluates surface fluxes in the $k = 3$ direction.
6. UPDATE advances the solution in time.

For efficiency of computation, Eq. (7) is coded in the following form

$$\begin{aligned} \bar{G}^{n+1} &= G^n - \frac{\omega \Delta t}{V} \left(\sum_k F \cdot S_k^+ + \sum_k F^- \cdot S_k^- \right) \\ G^{n+1} &= \bar{G}^{n+1} - \frac{\Delta t}{2V} \left[\left(\sum_k \bar{F}^+ \cdot S_k^+ + \sum_k \bar{F}^- \cdot S_k^- \right) \right. \\ &\quad \left. - (2\omega - 1) \left(\sum_k F \cdot S_k^+ + \sum_k F^- \cdot S_k^- \right) \right] \end{aligned} \quad (11)$$

so that instead of storing two time values of each variable, one time value and a flux accumulator are stored for each of the five dependent variables.

The flux calculations of the form $F \cdot S$ occur in pairs in Eq. (11) such that each of the FLUX(k) routines could be optimized in the k direction. For example, the $F \cdot S_k^+$ term for

one volume is the same as the $F^- \cdot S_k^-$ term for the adjacent volume. When these terms are summed in the k direction, unnecessary duplication of computations are avoided. This process is identical to MacCormack's split operator (Ref. 9), except that all fluxes are accumulated prior to updating.

The split coding necessitated that a pressure array be saved to avoid undesirable repetition of computations. For the same reason the volume and area vector arrays are also saved. Thus, 21 variables are stored for each mesh point. This number could be reduced by six if the area vectors from the mesh coordinates were recalculated as required, but the computation time would increase by about 25 percent.

Most of the results presented were obtained from the Cray-1 computer at United Computer Services, Kansas City. The Cray operating system contains a flow trace routine which monitors the time required in each subroutine. The resulting (mesh-dependent) timings are given in the following table:

<u>Routine</u>	<u>Percent of Time</u>
DTCAL	6
BC	17
FLUXX	16
FLUXY	13
FLUXZ	19
UPDATE	14
Other	15

A count of the number of operations per time step (predictor plus corrector) within FLUX(k) and UPDATE shows 112 floating point additions and 108 floating point multiplications per mesh point. Central processor time averages about 7×10^{-6} sec per mesh point per time step, depending on the mesh; this means the Cray-1 is operating at 50 million floating point operations per second when it is in these four routines.

3.0 RESULTS AND DISCUSSION

To ensure the accuracy and proper coding of the computer program, the flow field about several simple configurations was computed for comparison with results which have exact solutions. The geometries included a two-dimensional double-wedge and a cone at angle of attack at supersonic conditions. Two-dimensional planar (or axisymmetric) configurations are represented using one planar (or wedge-shaped) array of volume elements with symmetry boundary conditions on two sides.

Solutions were obtained for Mach number 2.0 flow over a 4.5-deg, double-symmetric wedge using two computational grids. A basically orthogonal mesh yields the results given in Fig. 2. Surface pressures are in good agreement with theory, but results within the flow field are not. Dispersion of the shock waves is evident, particularly so in the contour plot of constant pressure lines of Fig. 2b. Results obtained with the mesh aligned with the leading- and trailing-edge shocks are given in Fig. 3. The surface pressures are in excellent agreement with theory, and little dispersion or dissipation is evident. However, mesh alignment permits the appearance of an expansion shock emanating from the apex of the wedge. This phenomenon is attributable to the availability of an expansion shock as an exact solution to the Euler equations across one mesh boundary at the expansion location (Ref. 7). Some form of dissipation is necessary to prevent the occurrence of expansion shocks. Results obtained with third-order and explicit smoothing are presented in Fig. 4. It should be noted that the "omega factor" is nondissipative and thus has little effect on the expansion shock for this mesh.

Computations were also made for Mach number 2.0 flow over a 40-deg cone at 5-deg angle of attack. The computational mesh is illustrated in Fig. 5a, and an isobar contour plot is given in Fig. 5b. Some smearing of the bow shock is apparent. Stability problems were encountered with the cone mesh configuration so that smoothing was mandatory. Surface pressure results are given in Fig. 5c for both the mesh of Fig. 5a and for a coarser mesh containing only nine circumferential elements. Both solutions are in good agreement with the results of Jones (Ref. 10). However, detailed examination of the solutions shows the fine-mesh solution with less than twice the number of points to be about five times more accurate than the coarse mesh solution.

It is relatively easy to incorporate streamline curvature effects in the surface boundary condition for simple configurations. Computations have been made for a 1.5-caliber ogive-cylinder at 20-deg angle of attack with both mirror and the normal momentum equation surface boundary conditions. The results are given in Fig. 6, along with experimental data from Ref. 11. Cross flow separation occurs at $x/D \approx 4.5$ (off the figure scale) which, of course, cannot be predicted using the Euler equations. Before separation, the computations and experimental data are in reasonably good agreement.

Although only speculation at present, the error introduced through use of the mirror boundary condition appears to create effective vorticity and a corresponding stagnation pressure loss that bears some resemblance to true viscous effects. For example, calculations indicate a 5-percent loss in stagnation pressure close to the ogive-cylinder body at $x/D = 2$ which increases to 10-percent loss at $x/D = 10$. The loss is circumferentially uniform close to the nose but then convected to the leeward side, as expected of viscous effects. Users of

the code should routinely compute and examine both stagnation pressure and enthalpy distribution throughout the flow field to evaluate solution accuracy.

An example of the program's flexibility is indicated by the mesh in Fig. 7a for computing the flow over three separated aircraft stores in a triple-ejection-rack configuration. The mesh consists of two distinct computational grids interconnected by the boundary condition routine, which required the addition of only 35 FORTRAN statements to the basic computer program. A comparison of computed results with the experimental surface pressure data of Heltsley and Cline (Ref. 12) is given in Fig. 7b. Note that the flow in the gap between the stores is locally supersonic. Computations at a free-stream Mach number of 0.9 (not shown) indicate two strong shocks in the gap.

As a precursor to the development of a three-dimensional wing/cascade version of ARO-1, solutions have been obtained for a two-dimensional lifting airfoil. The calculations are compared with the experimental data of Ref. 11 in Fig. 8. The trailing-edge boundary condition was simply continuity of dependent variables across the "wake." The lack of agreement between the computations and experiment, particularly at supercritical conditions, is unexplained. However, these differences are quite similar to the effects of wind tunnel wall interference illustrated in Ref. 11.

Computation of flow over an F-16 aircraft forebody (including strakes but, as yet, without inlet flow) provides a three-dimensional example. The computational mesh in the vertical plane is given in Fig. 9a, and a comparison of computed results with experimental pressure data along the top surface is presented in Fig. 9b. Considering the relative coarseness of the mesh, these results clearly show the general applicability of ARO-1 to this class of configurations.

Use of the Euler equations rather than the potential flow assumption permits calculation of rotational flows such as secondary flow induced in curved ducts. Such a calculation can be applied in the contraction section of a wind tunnel. The outermost part of the computational mesh for a contraction with transition from a circular to a rectangular to a square cross section is illustrated in Fig. 10a, with the interior mesh at the upstream cross section given in Fig. 10b. With uniform flow at the inlet, the exit flow is contaminated by small secondary flows, as shown by the cross flow velocity vectors in Fig. 10c. The maximum magnitude of the corresponding flow angularity is 0.1 deg.

Another example of a curved duct computation is given in Fig. 11. An aircraft engine-inlet duct is modeled with transition from an elliptic to a circular cross section with a mild centerline offset. Note the replicated mesh points at the duct centerline in Fig. 11b and recall

that the finite volume formulation does not permit flux through a surface of zero area. Nonetheless, computed results such as those given in Fig. 11c appear reasonable and are in good qualitative agreement with experimental data.

A final example of code flexibility is provided by solutions of an axisymmetric flow over a hollow-nose infrared sensing probe as shown in Fig. 12a. The mesh (Fig. 12b) was generated by a variant of Thomas' approach (Ref. 13) which solves two coupled Poisson equations to yield interior mesh coordinates from specified boundary coordinates. Computed isobars for steady flow at $M_\infty = 1.35$ are given in Fig. 12c. The explicit smoothing added to maintain stability tends to smear the bow shock over several mesh points. Cancellation of the shock at the mesh boundary was obtained using zero normal gradient boundary conditions.

Time-accurate unsteady flow can also be calculated, as evidenced by the sequence of isobar plots in Fig. 13 resulting from the introduction of a planar blast wave upstream of the infrared sensing probe. Shock-shock interactions and multiple shock reflections pose no computational difficulties, although the accuracy of the computations is unknown, except to note that the blast wave speed was correctly represented.

The probe was to be cooled by injecting air in the cavity. A solution was obtained with, in effect, counter-flowing cold jets by local modification of the surface boundary condition to permit blowing. Isobars of the resulting solution are given in Fig. 14a, and the path of the "coolant" is indicated by lines of constant temperature in Fig. 14b. The face of the probe cannot be cooled by this technique.

4.0 CONCLUDING REMARKS

A generalized computer program for solution of the three-dimensional, unsteady Euler equations has been developed. Selection of the finite-volume approach in Cartesian coordinates yielded a flexible code capable of treating arbitrary model geometry, including both internal and external flow configurations. Efficient coding and use of the Cray-1 computer enables reasonably short solution times on fairly complex and dense meshes.

Development of the code is providing even greater flexibility and extending the number of model flow configurations that can be computed on a routine basis. For example, viscous-inviscid interactions can be computed approximately through incorporation of an inverse, two-dimensional strip, boundary-layer method (Ref. 14) which requires modification of only the boundary condition routine. That code is designated ARO-2.

REFERENCES

1. Jameson, A. and Caughey, D. A. "A Finite-Volume Method for Transonic Potential Flow Calculations." Proceedings of AIAA 3rd Computational Fluid Dynamics Conference, Albuquerque, New Mexico, June 27-28, 1977.
2. Caughey, D. A. and Jameson, A. "Numerical Calculation of Transonic Potential Flow About Wing-Body Combinations." AIAA Paper No. 77-677, June 1977.
3. Caughey, D. A. and Jameson, A. "Recent Progress in Finite-Volume Calculations for Wing-Fuselage Combinations." AIAA Paper No. 79-1513, July 1979.
4. Boppe, C. W. and Stern, M. A. "Simulated Transonic Flows for Aircraft with Nacelles, Pylons, and Winglets." AIAA Paper No. 80-0130, January 1980.
5. Cline, M. C. "NAP: A Computer Program for the Computation of Two-Dimensional, Time-Dependent, Inviscid Nozzle Flow." Los Alamos Scientific Laboratory, LA-5984, January 1977.
6. MacCormack, R. W. "The Effect of Viscosity in Hypervelocity Impact Cratering." AIAA Paper No. 69-354, May 1969.
7. MacCormack, R. W. and Paullay, A. J. "The Influence of the Computational Mesh on Accuracy for Initial Value Problems with Discontinuous or Nonunique Solutions." *Computers and Fluids*, Vol. 2, 1974.
8. Jacocks, J. L. "Computation of Axisymmetric Separated Nozzle-Afterbody Flow." AEDC-TR-79-71 (AD-A079694), January 1980.
9. MacCormack, R. W. and Paullay, A. J. "Computational Efficiency Achieved by Time Splitting of Finite Difference Operators." AIAA Paper No. 72-154, January 1972.
10. Jones, D. J. "Numerical Solution of the Flow Field for Conical Bodies in a Supersonic Stream." National Aeronautical Establishment, NRC No. 10361, July 1968.
11. Barche, J., et al. "Experimental Data Base for Computer Program Assessment." AGARD-AR-138, May 1979.
12. Heltsley, F. L. and Cline, V. A., Jr. "Wing/Store Flow Field Measurement at Transonic Speeds Using a Laser Velocimeter." AEDC-TR-79-5 (AD-A068328), April 1979.
13. Thomas, P. D. "Numerical Method for Predicting Flow Characteristics and Performance of Nonaxisymmetric Nozzles — Theory." NASA Contractor Report 3147, September 1979.

14. Whitfield, D. L., Swafford, T. W., and Jacocks, J. L. "Calculation of Turbulent Boundary Layers with Separation, Reattachment, and Viscous-Inviscid Interaction." AIAA Paper No. 80-1439, July 1980.

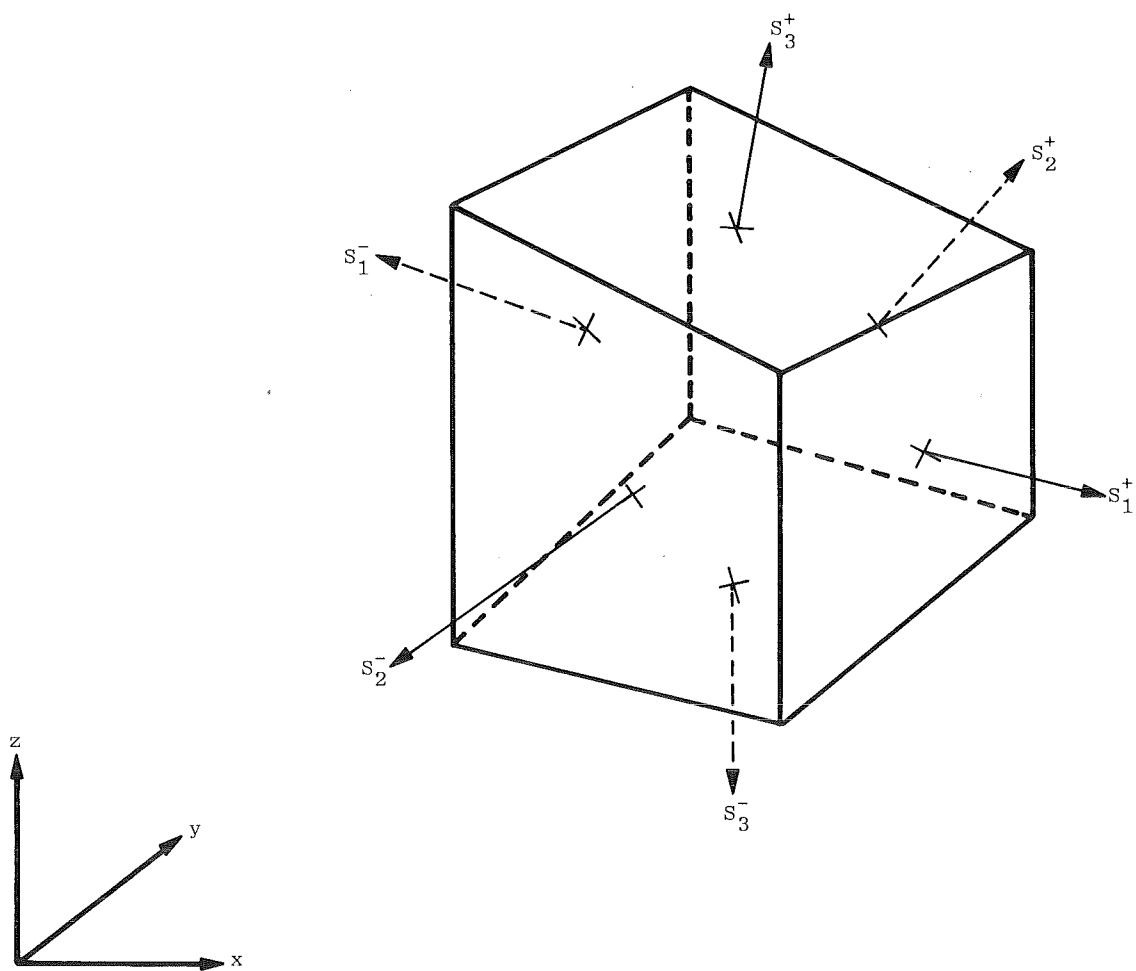
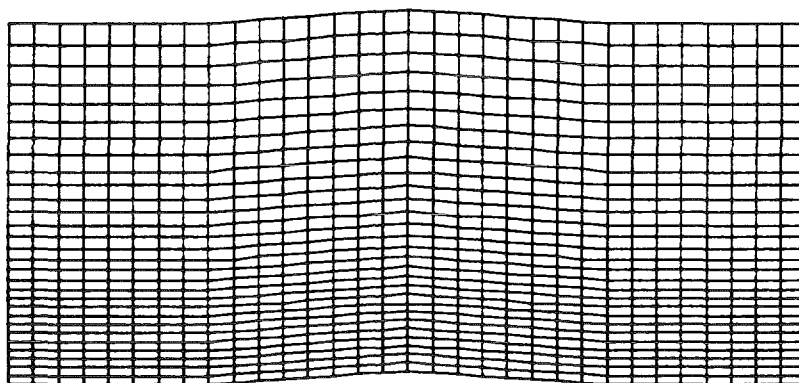
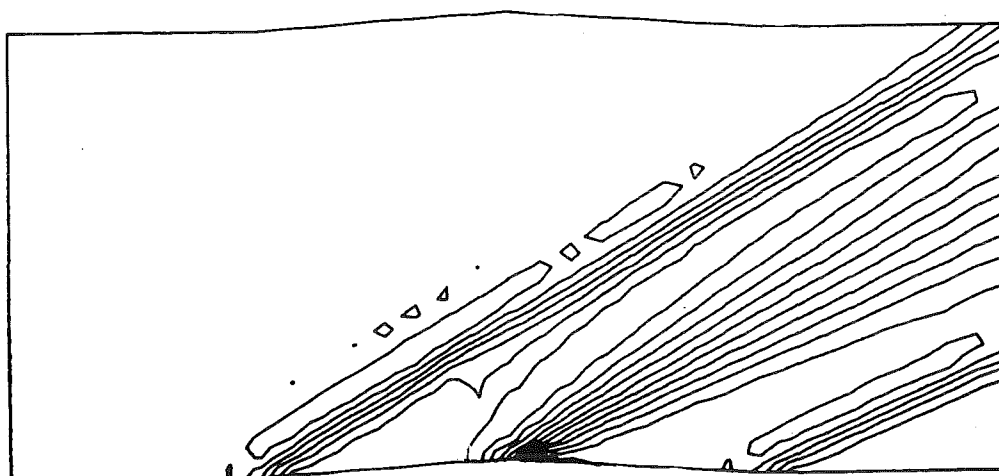


Figure 1. Computational mesh nomenclature.

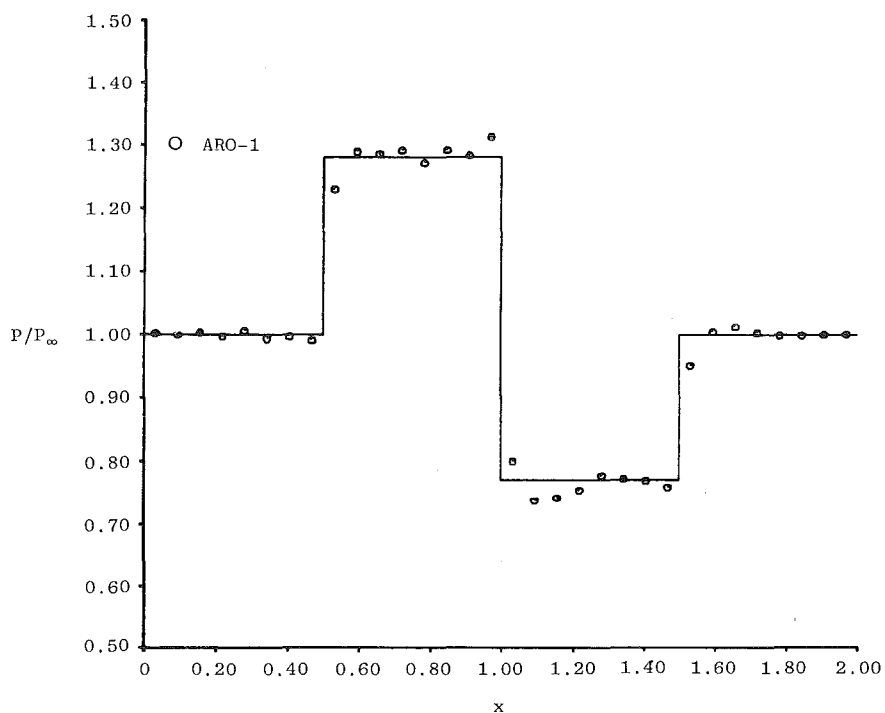


a. Computational mesh

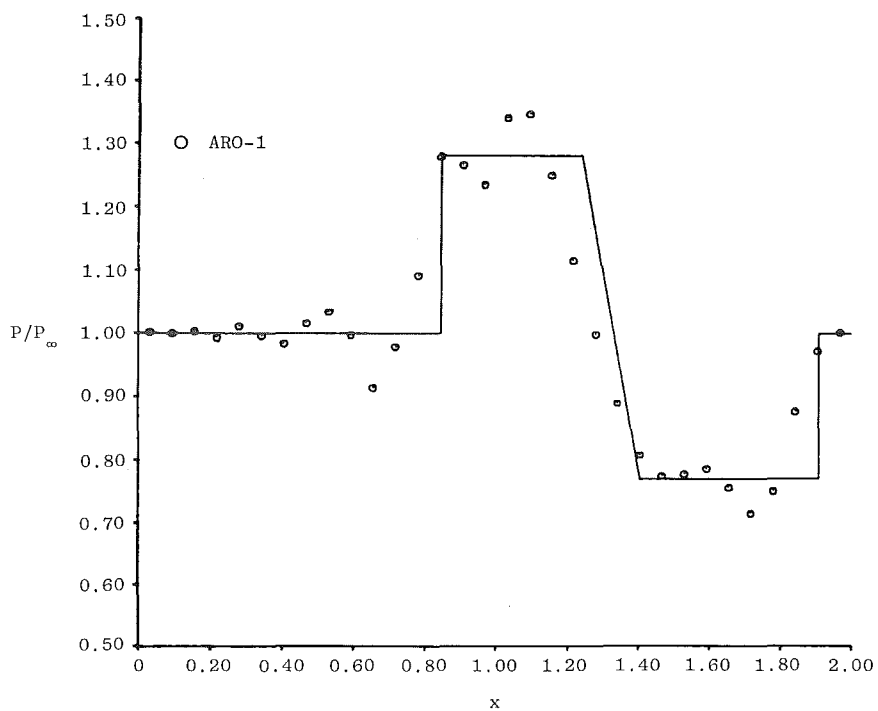


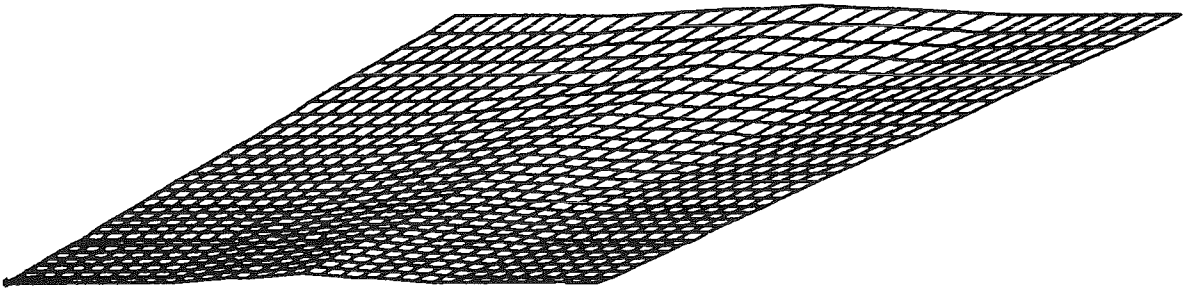
b. Isobars

Figure 2. Computation of flow over a double-wedge with orthogonal mesh.

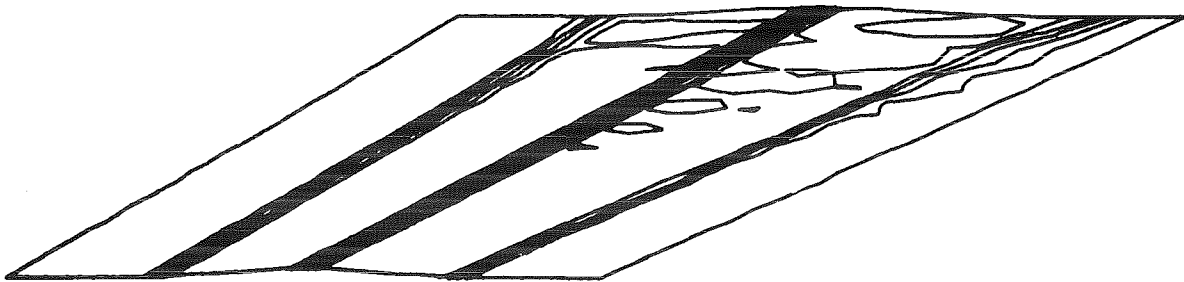


c. Surface pressure

d. Pressure at $y = 0.2$
Figure 2. Concluded.

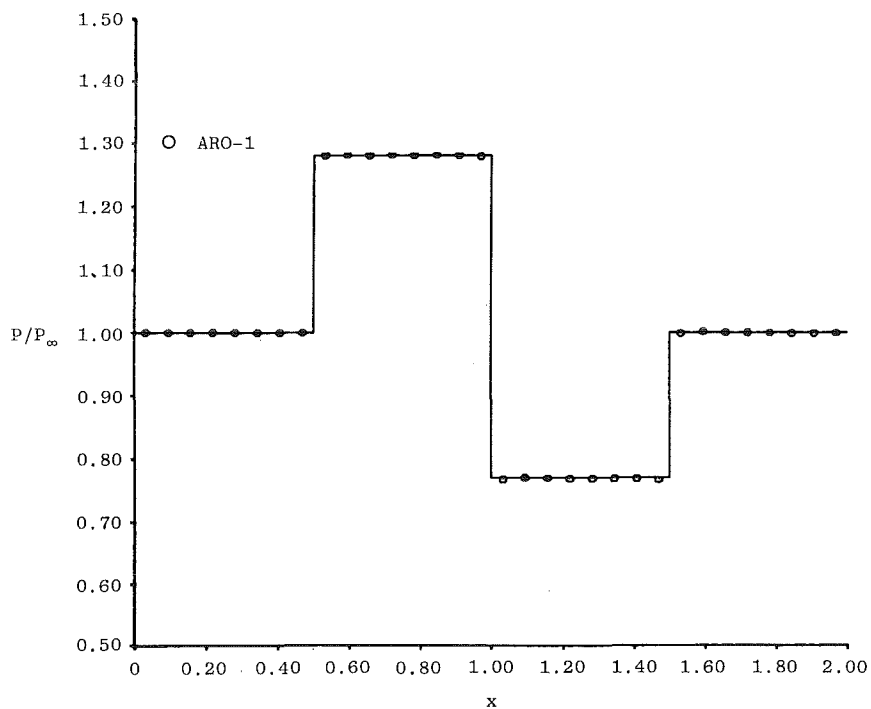


a. Computational mesh



b. Isobars

Figure 3. Computation of flow over a double-wedge with inclined mesh.



c. Surface pressure

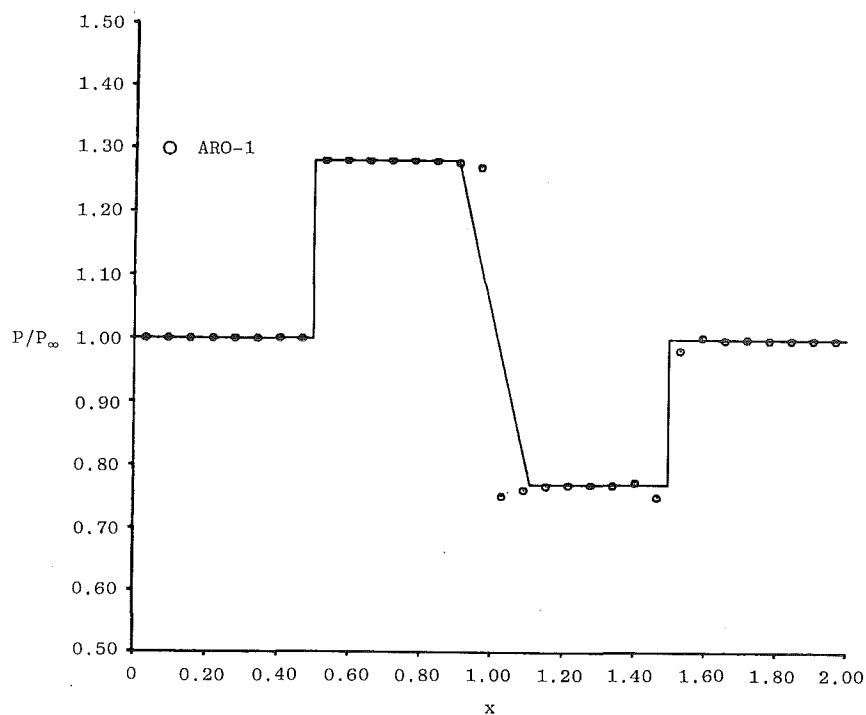
d. Pressure at $y = 0.2$

Figure 3. Concluded.

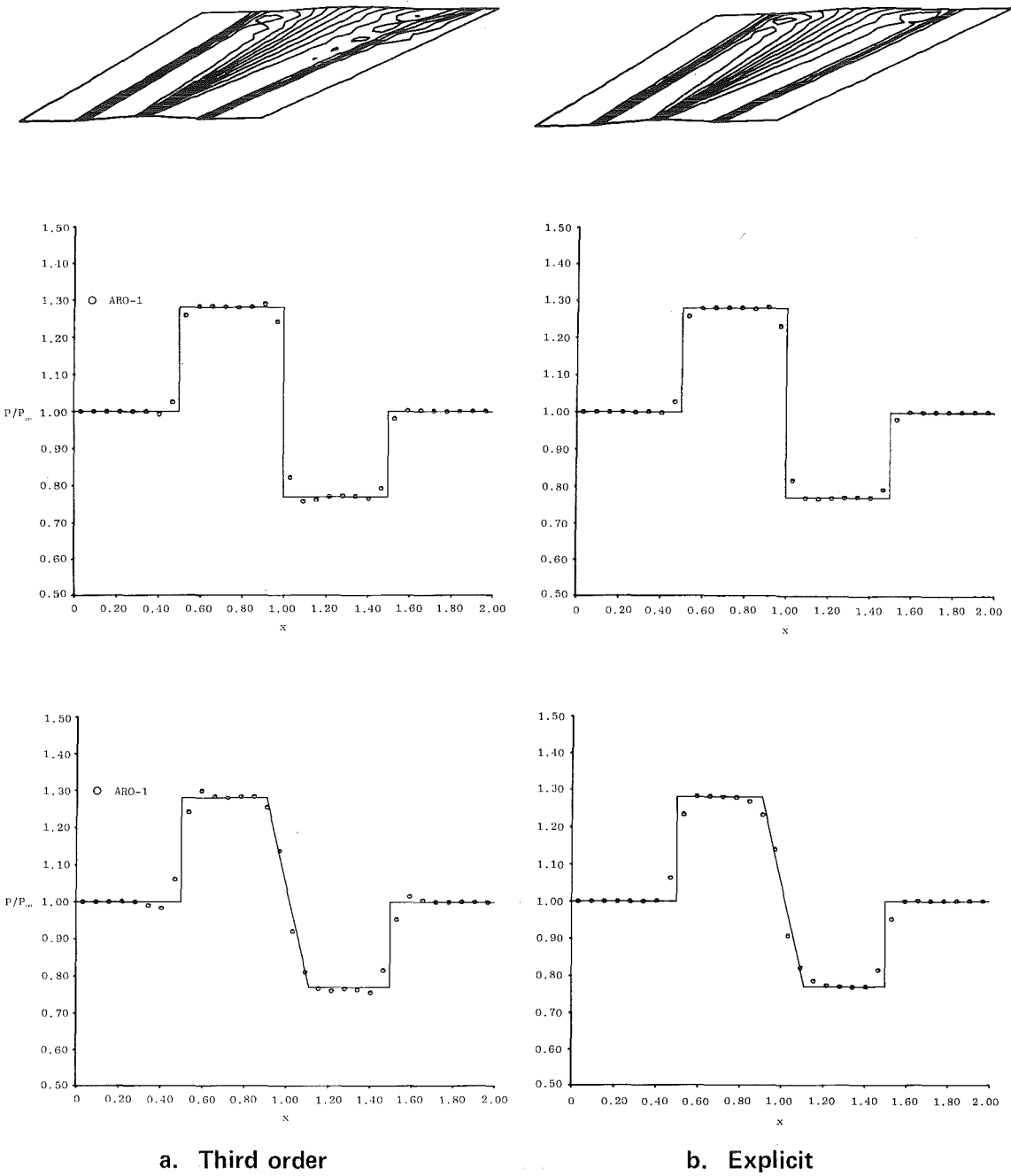
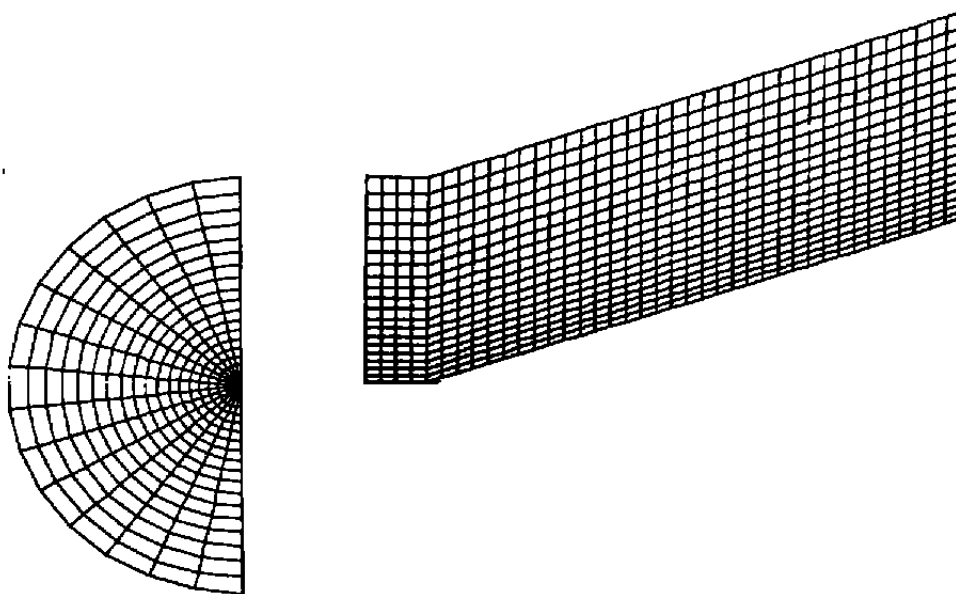
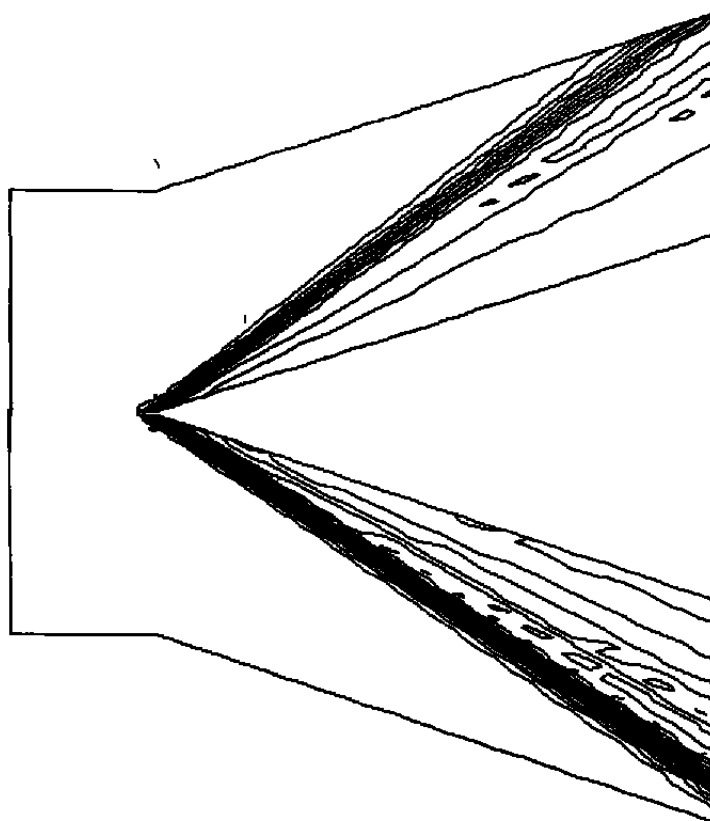


Figure 4. Effect of smoothing.

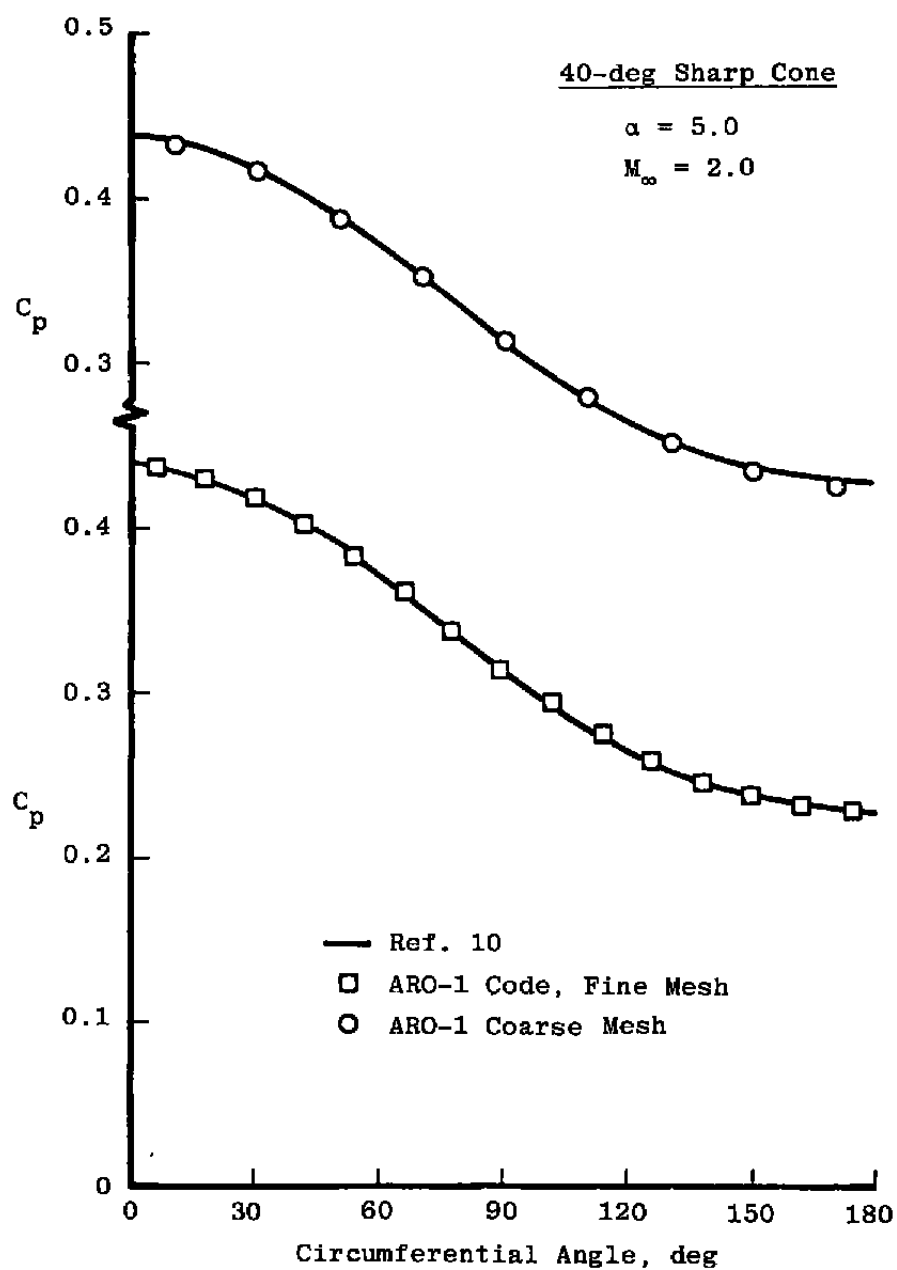


a. Computational mesh



b. Isobars

Figure 5. Computation of flow over a cone at angle of attack.



c. Surface pressure
Figure 5. Concluded.

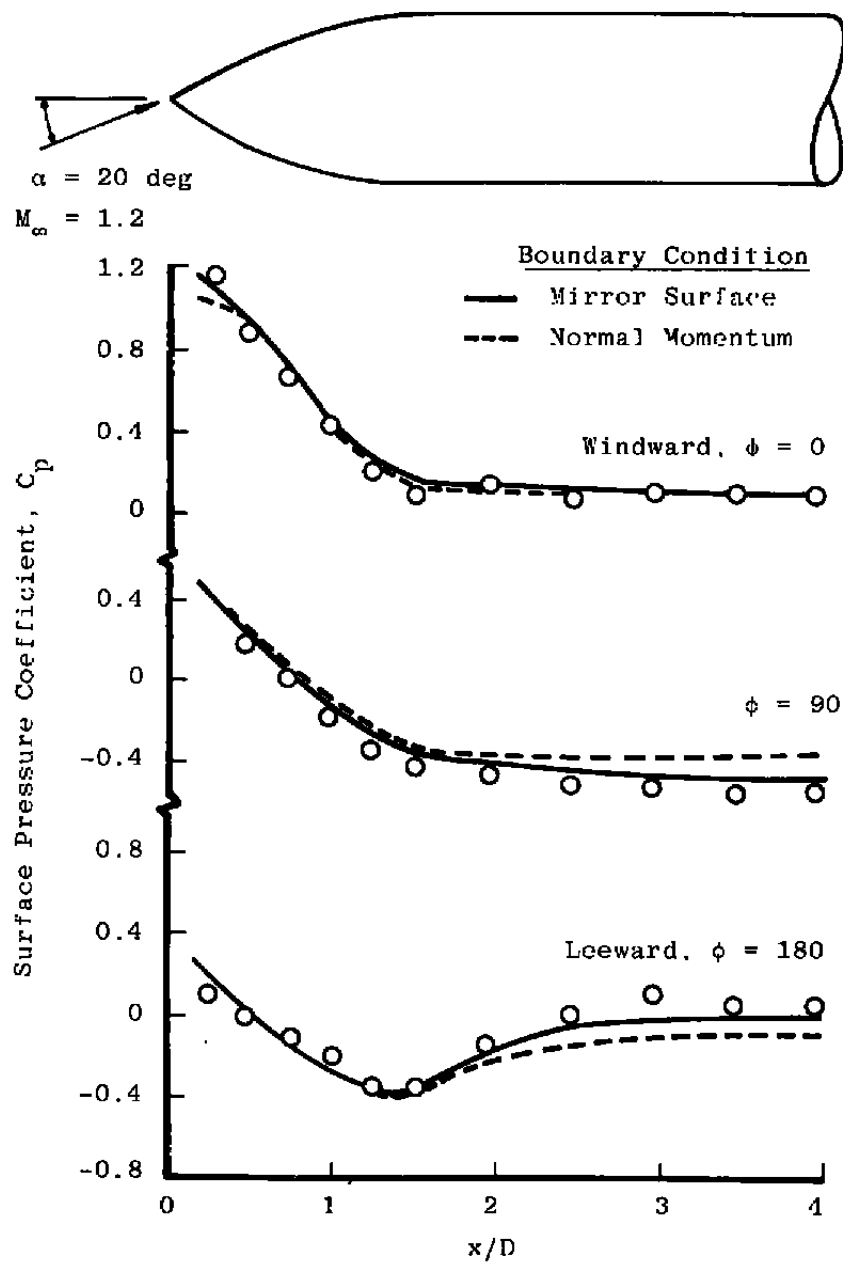
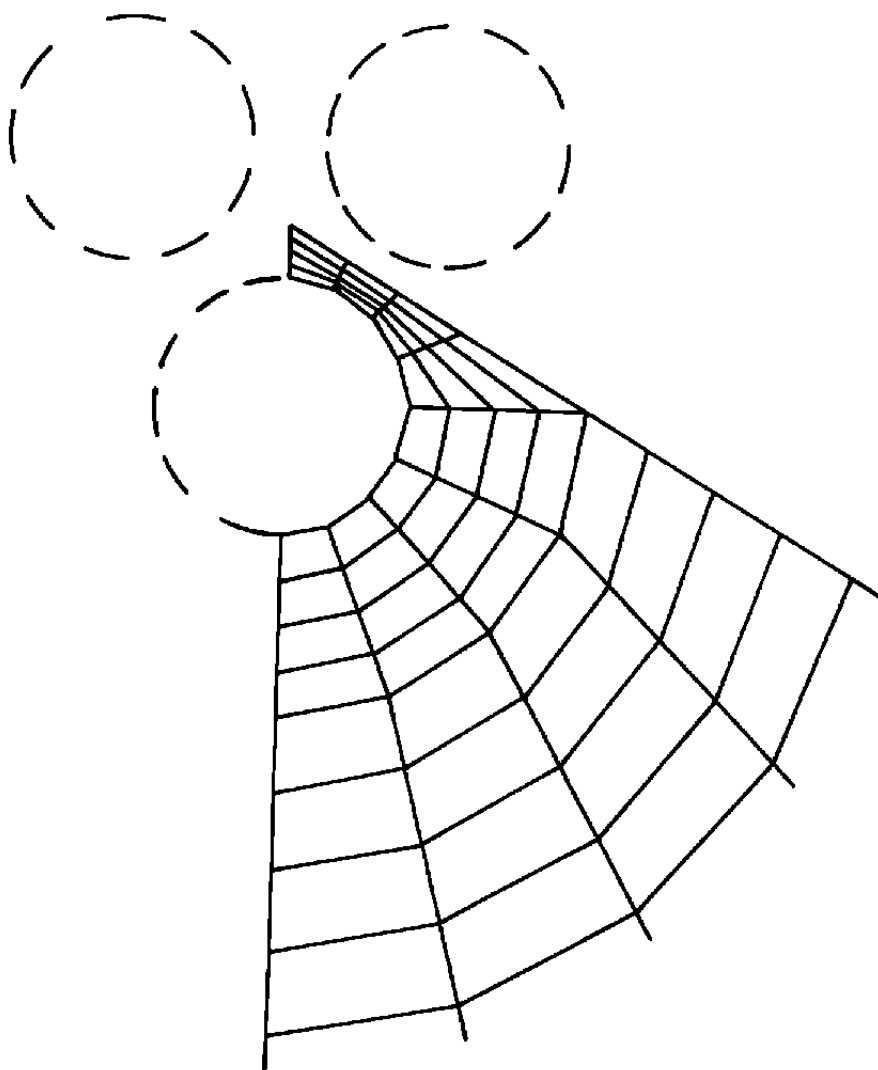
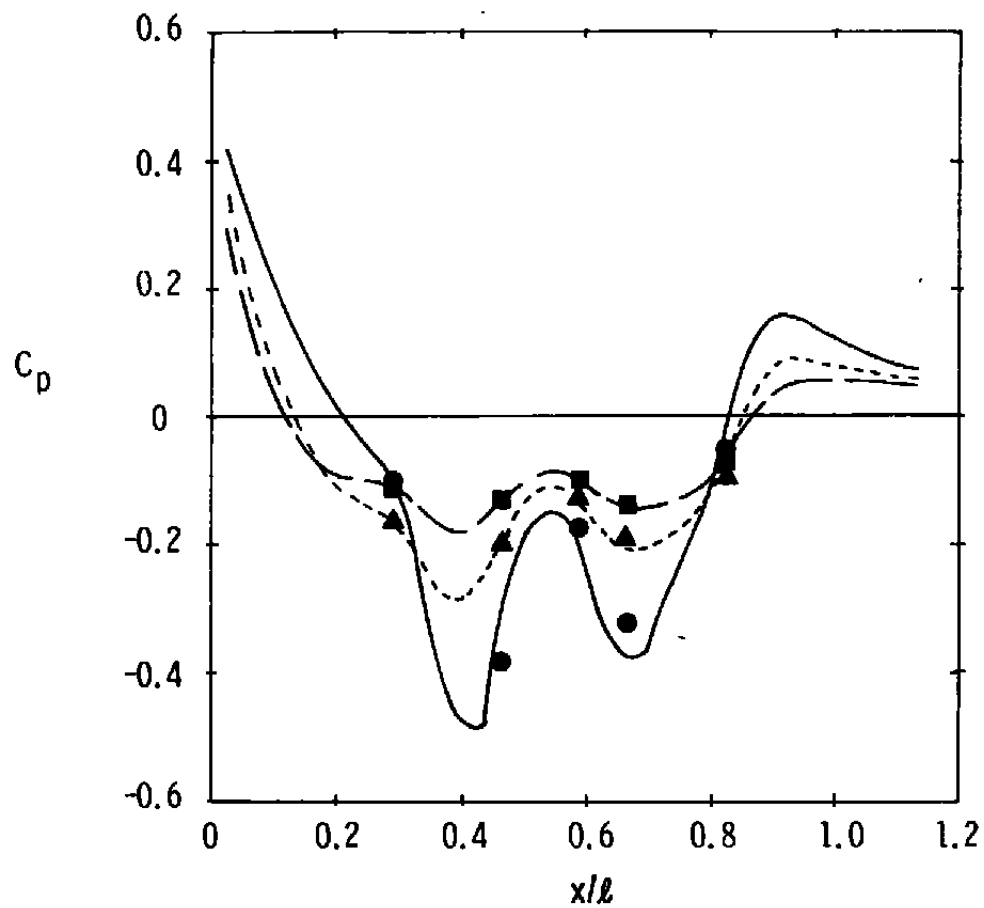


Figure 6. Computation of flow over an ogive-cylinder at angle of attack.

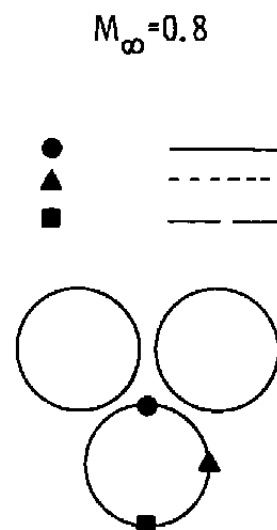


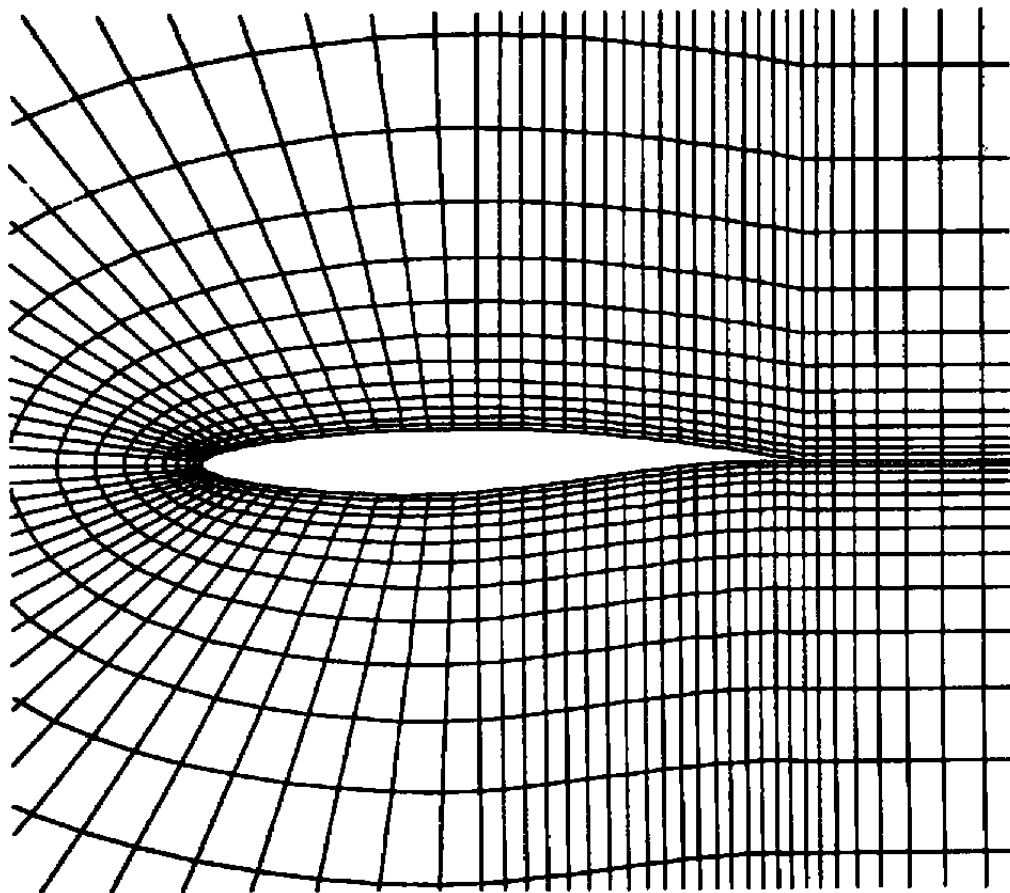
a. Computational mesh

Figure 7. Computation of flow over a three-store cluster at zero angle of attack.



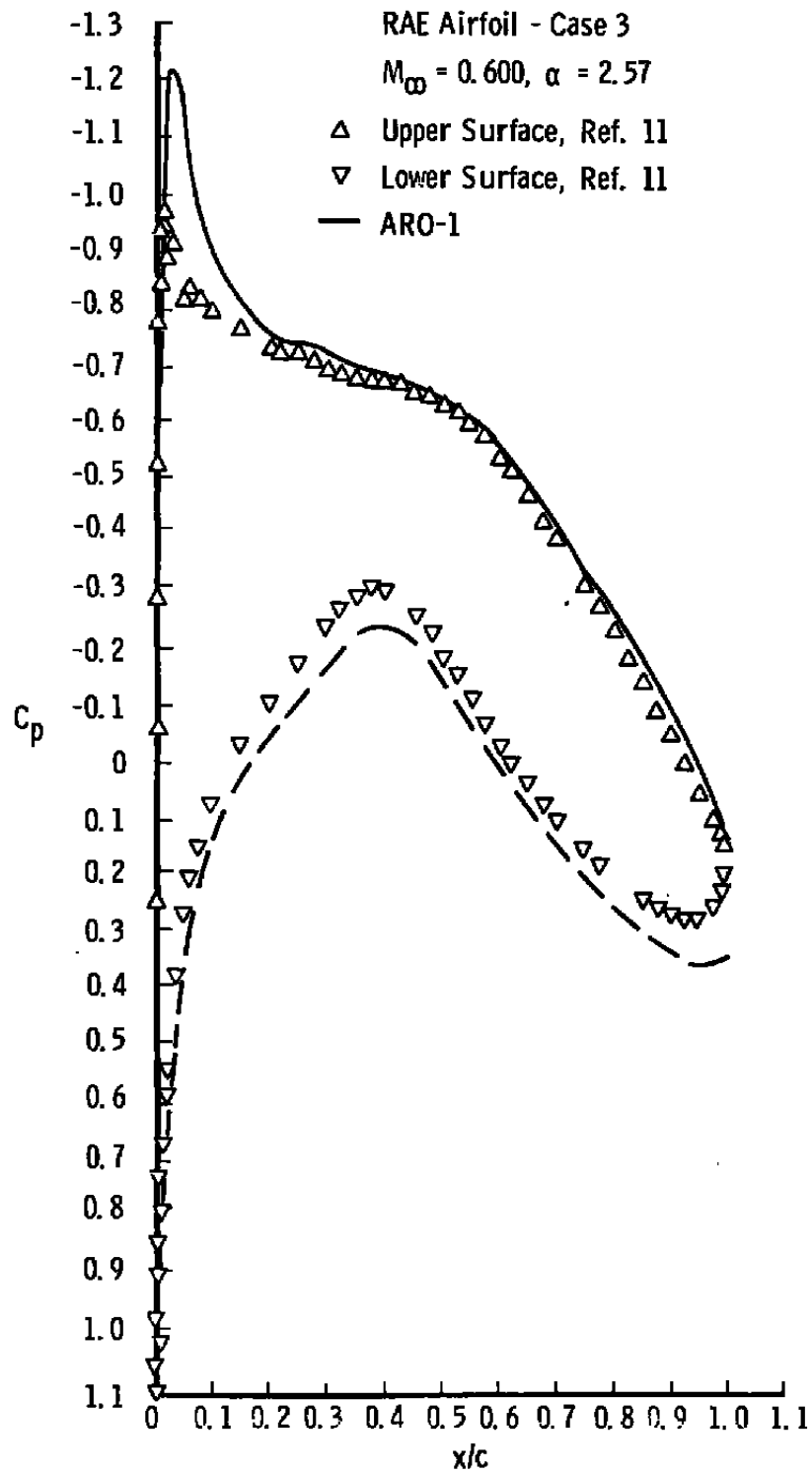
b. Surface pressure results
Figure 7. Concluded.



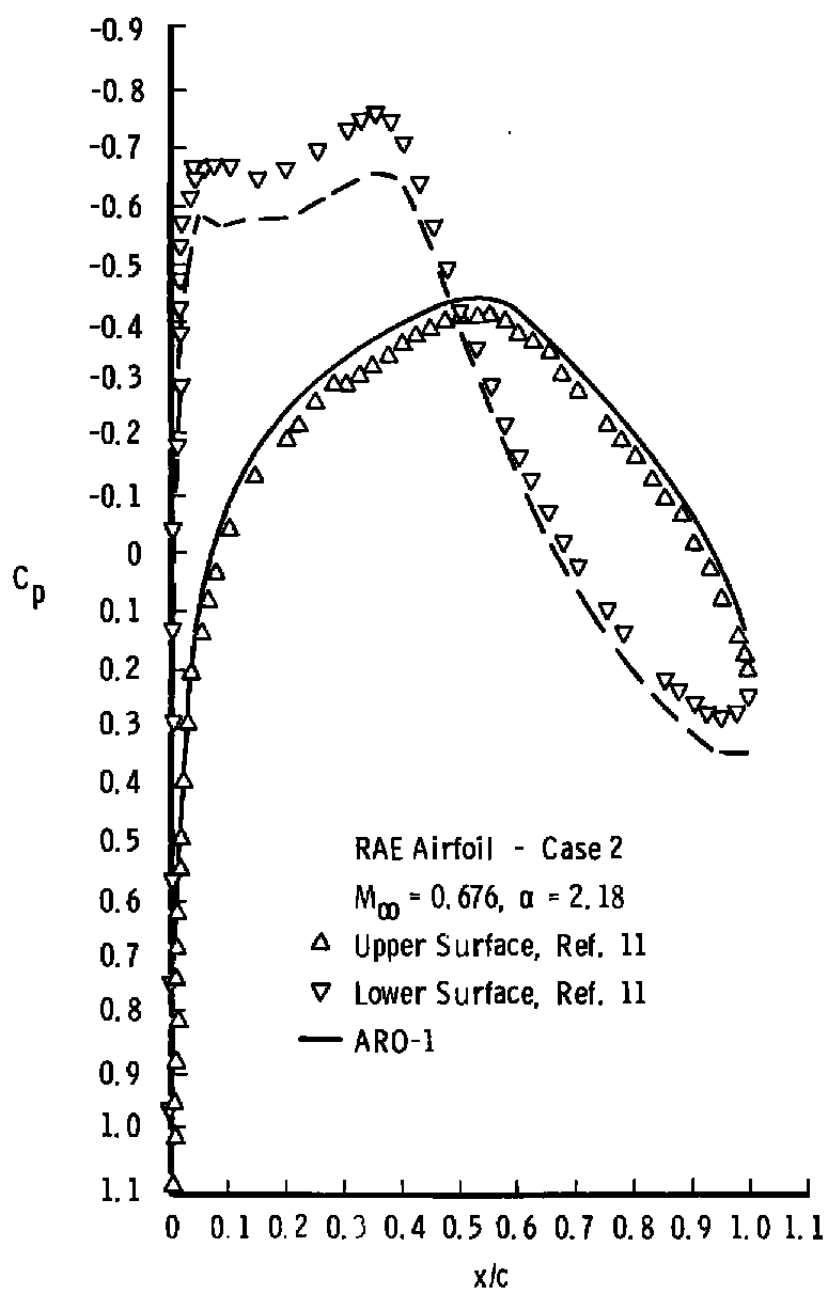


a. Computational mesh

Figure 8. Computation of flow over a lifting airfoil.



b. Surface pressure, $M_\infty = 0.6$
 Figure 8. Continued.



c. Surface pressure, $M_\infty = 0.676$
 Figure 8. Continued.

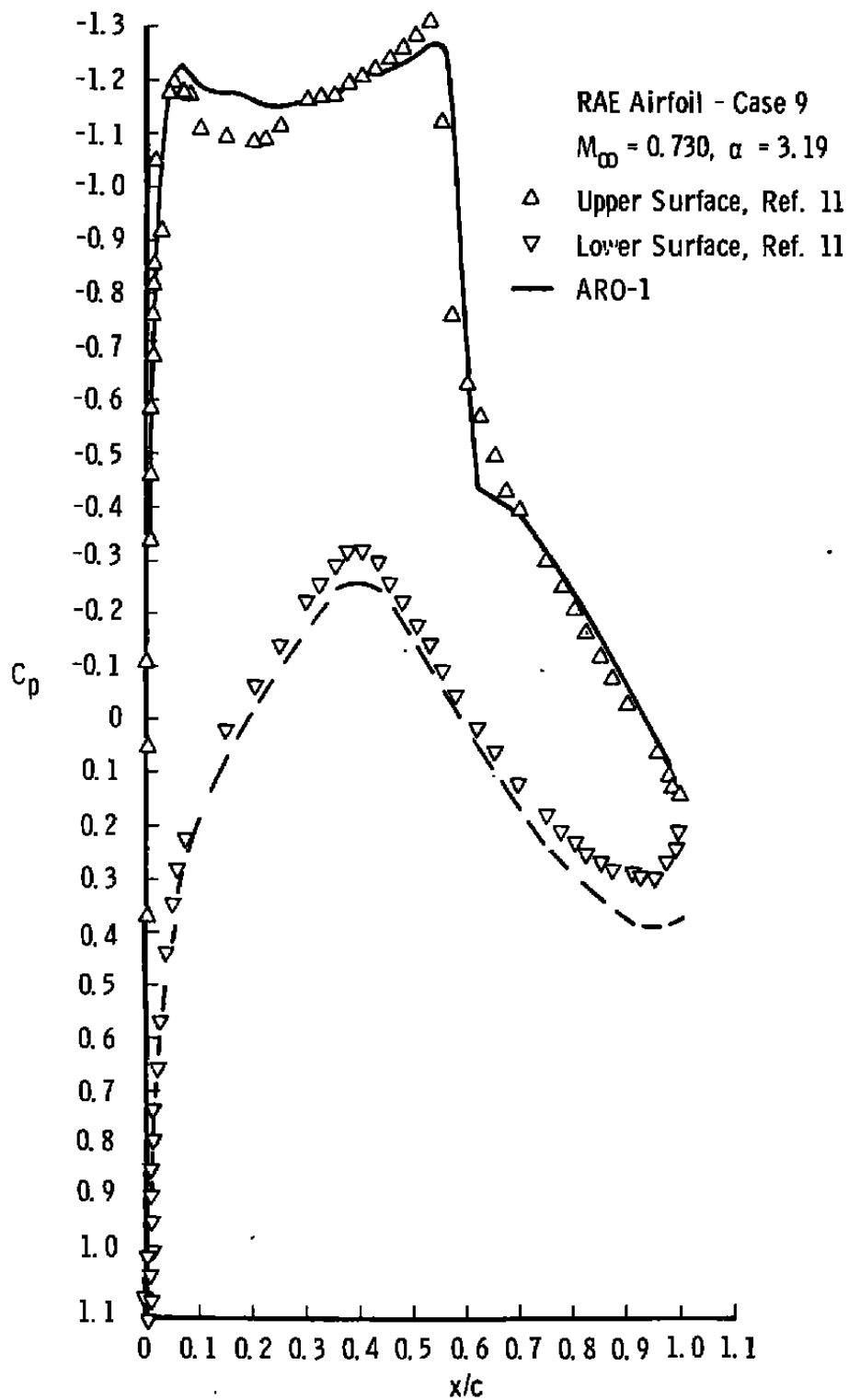
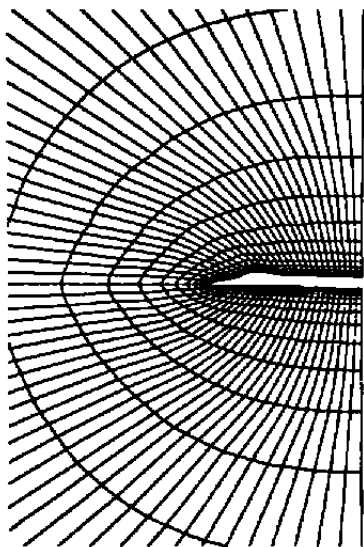
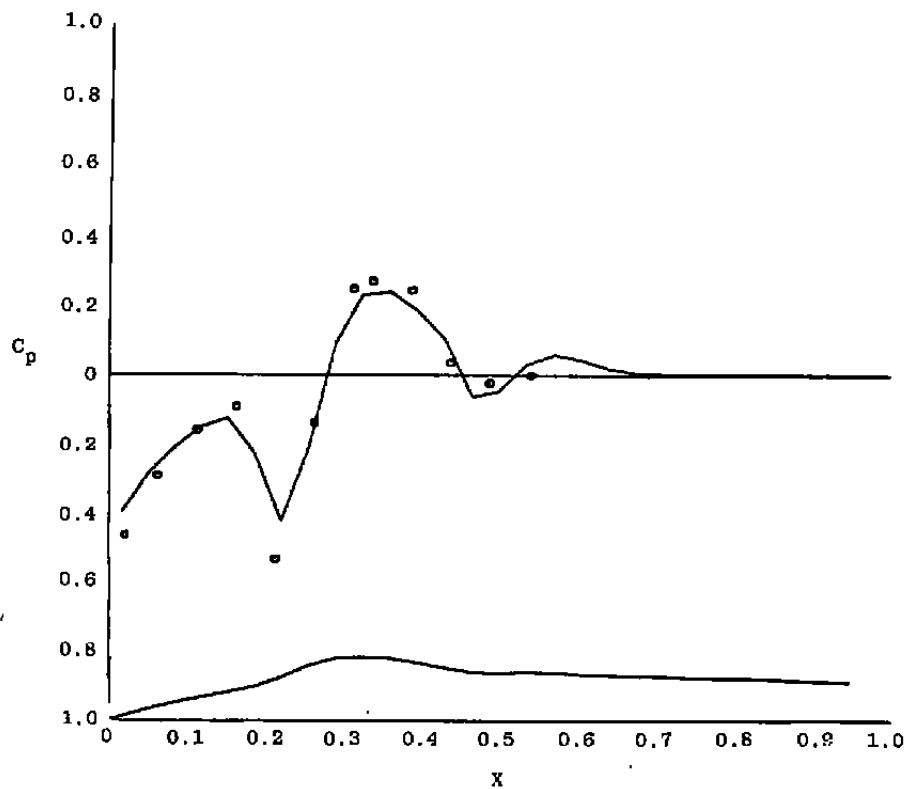
d. Surface pressure, $M_{\infty} = 0.73$

Figure 8. Concluded.

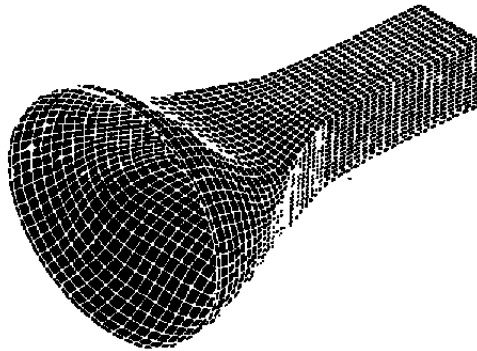


a. Computational mesh

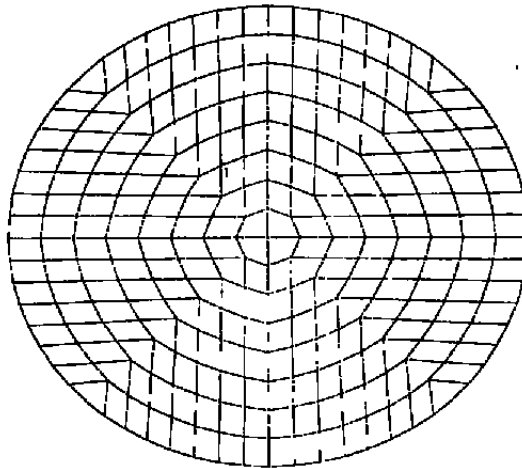


b. Surface pressure

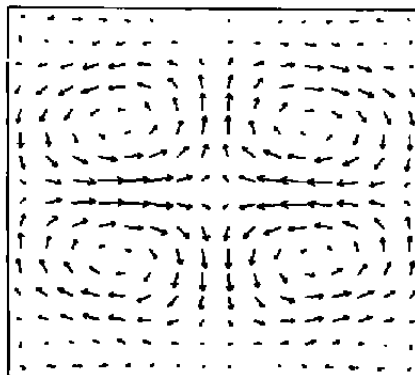
Figure 9. Computation of flow over an aircraft forebody.



a. Duct geometry

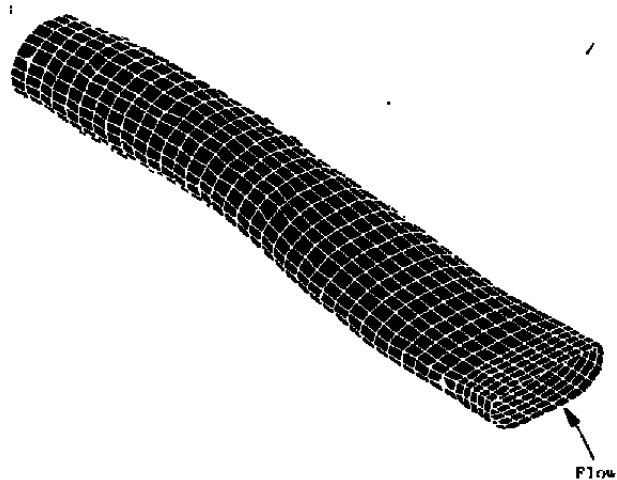


b. Upstream mesh cross-section

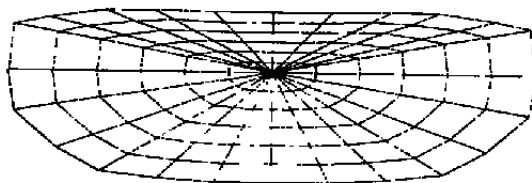


c. Exit plane velocity vectors

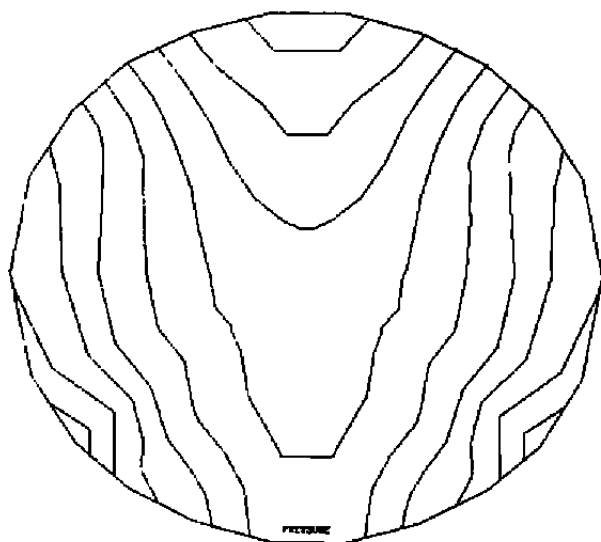
Figure 10. Computation of flow within a wind tunnel contraction.



a. Duct geometry

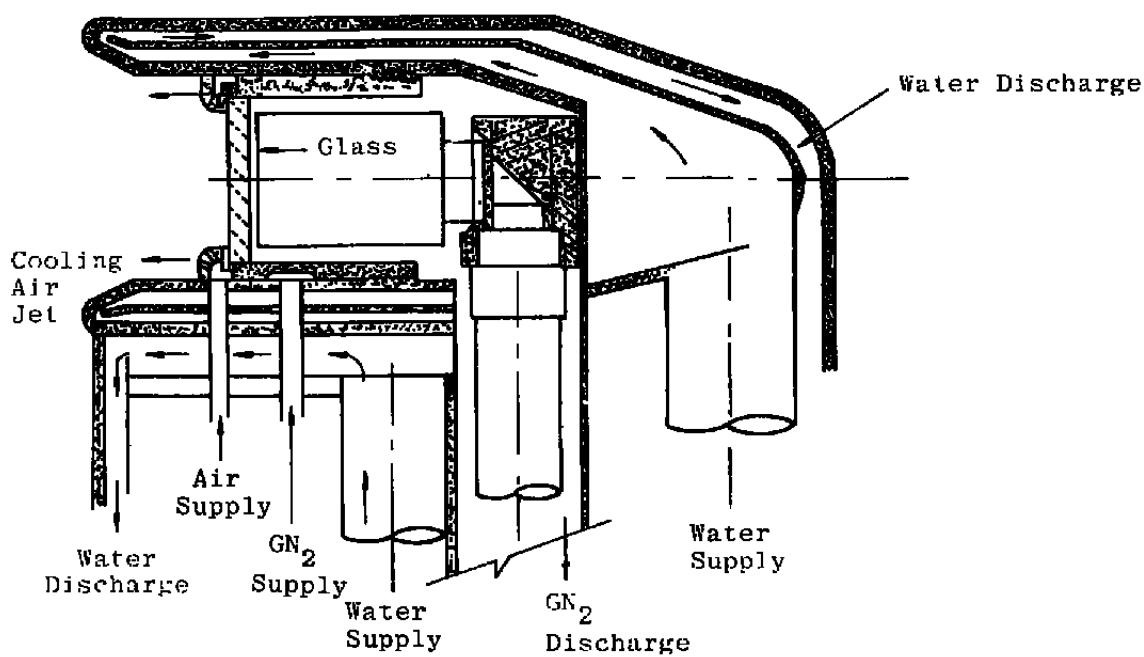


b. Interior mesh at the upstream cross-section

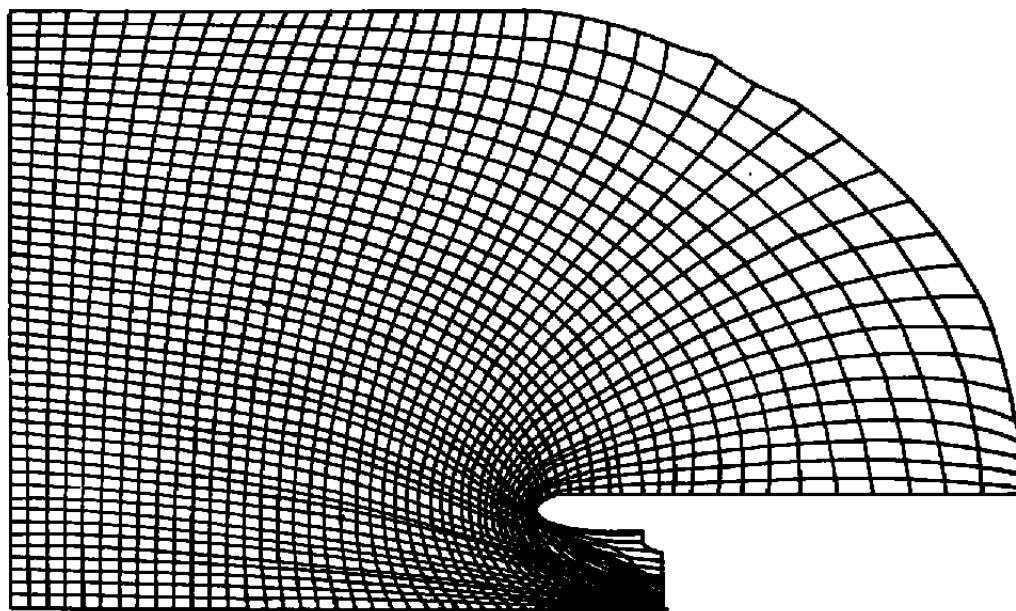


c. Contours of constant stagnation pressure
at engine inlet

Figure 11. Computation of flow within an aircraft inlet.

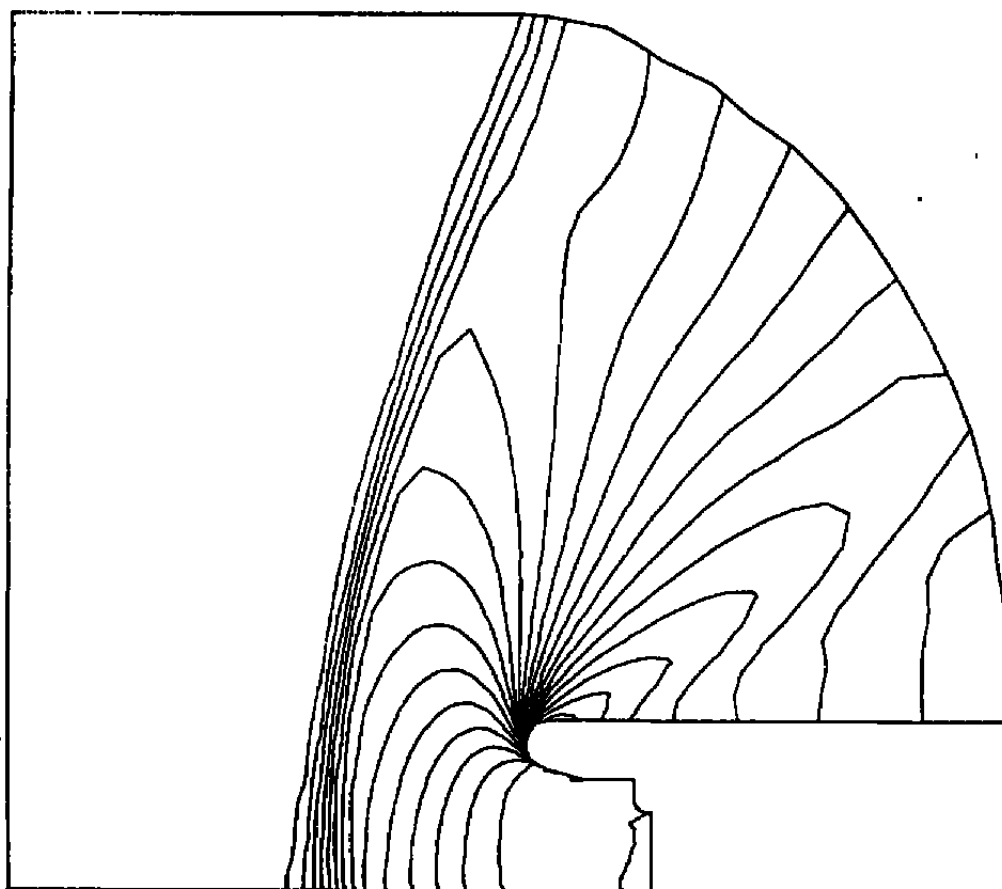


a. Probe geometry

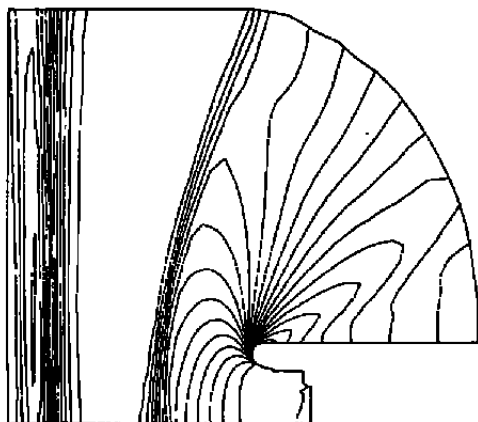


b. Computational mesh

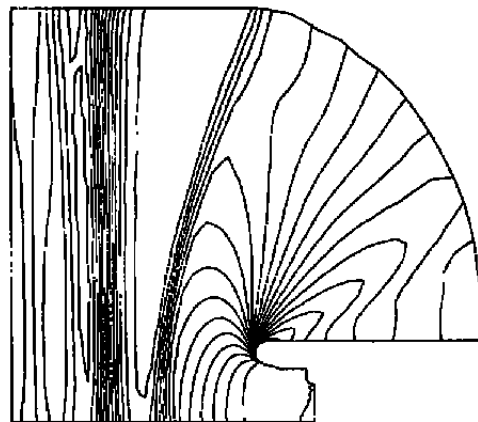
Figure 12. Computation of flow about a hollow-nose probe.



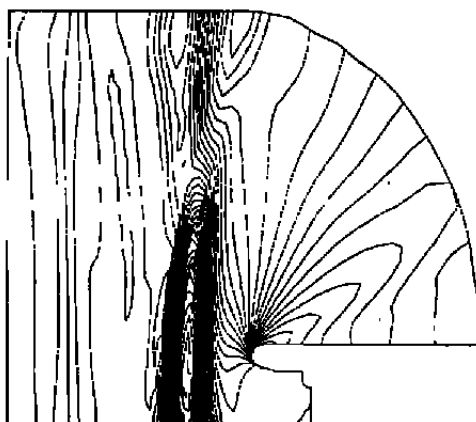
c. Isobars
Figure 12. Concluded.



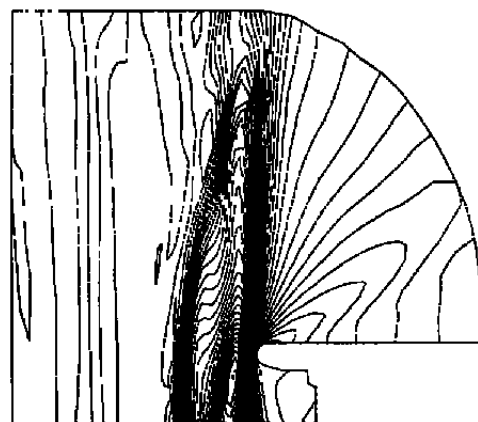
a. Time = Δt



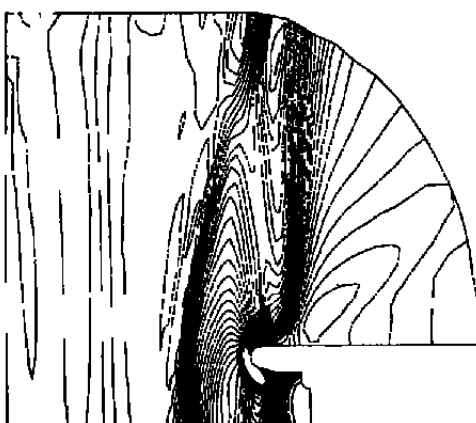
b. Time = $2 \Delta t$



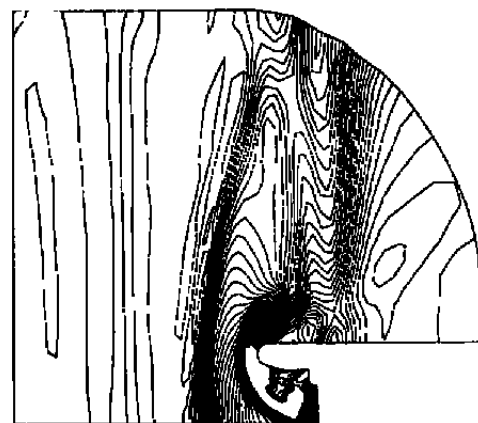
c. Time = $3 \Delta t$



d. Time = $4 \Delta t$

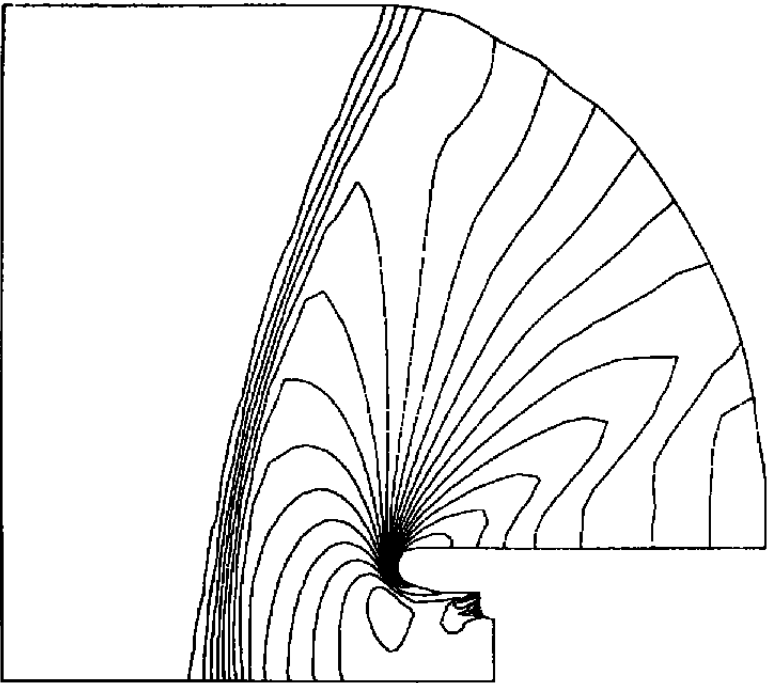


e. Time = $5 \Delta t$

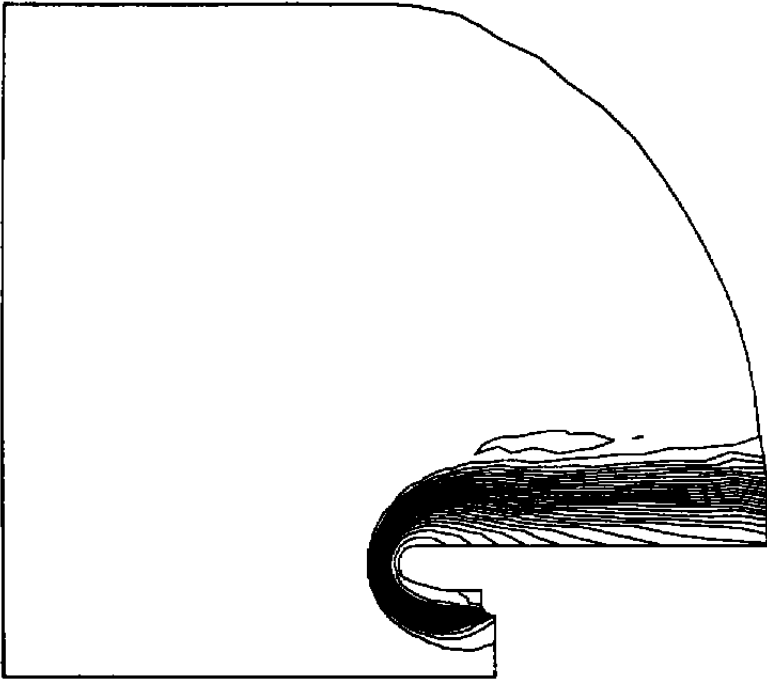


f. Time = $6 \Delta t$

Figure 13. Computation of unsteady flow.



a. Isobars



b. Lines of constant temperature

Figure 14. Computation of counter-flowing jets.

NOMENCLATURE

c	Sound speed
D	Diameter
e	Specific energy
F	Tensor of independent variables defined in Eq. (2)
G	Vector of dependent variables, Eq. (2)
k	Direction index
n	Unit-normal vector
P	Pressure
q	Velocity vector
S	Surface
S_k	Surface area vector
t	Time
u	Velocity in x-direction
V	Volume
v	Velocity in y-direction
W	Weighting factor, Eq. (10)
w	Velocity in z-direction
x,y,z	Cartesian coordinates
α	Angle of attack
γ	Ratio of specific heats
ρ	Density
ϕ	Roll orientation
ω	Stabilization parameter in Eq. (7)

SUBSCRIPTS

bc	Boundary condition
in	Interior
k	Direction index
max	Maximum
min	Minimum
∞	Free-stream conditions

SUPERSCRIPTS

n	Time index
+	Positive direction sense
-	Negative direction sense
overbar	Predictor time level